Check for updates

High barrier bio-nanocomposite films of ethyl cellulose integrated with modified nanocellulose: effect of nanocellulose's substituted side chains on film performance†

Supattra Klayya,[a] Patcharee Pripdeevech,[a,b] Emiliano Bilotti,[c] Han Zhang [ID][d] and Nattakan Soykeabkaew*[a,e]

Bio-based packaging films with good barrier properties to preserve quality, ensure safety, and extend the shelf-life of food products are in great demand as our society becomes more environmentally conscious. Herein, entirely bio-based nanocomposite films of the ethylcellulose (EC) matrix, reinforced with modified nanofibrillated cellulose (mNFC), have been studied. The NFC modification consisted in a microwave-assisted esterification reaction with three different acids – lactic acid (LA), lauric acid (LU), and stearic acid (SA) – of varying carbon chain lengths, in three solvents (water, ethanol, and ethyl acetate). The highest degree of substitution (DS) for mNFC-LA was achieved in ethanol, while mNFC-LU and mNFC-SA showed the maximum DS (up to 1.22) in ethyl acetate. The success of NFC surface modification was confirmed by titration, FTIR, XRD, SEM, and nanocellulose dispersion behavior. The films of EC-based nanocomposites were prepared by solvent casting and then examined for surface morphology, microstructures, mechanical properties, surface properties and barrier properties against water vapor and oxygen transmission. The findings revealed that integrating mNFC into EC can greatly improve the properties of the films due to their good compatibility, good dispersion ability, and strong interface, which is influenced by the substituted side chain on the mNFC surface. For the best side chain length (3 carbon atoms), mNFC-LA increased the tensile strength of the EC film by up to 130% while reducing the oxygen transmission rate (OTR) by 98%, making it a viable and environmentally benign alternative to PET films. This research offers insights into employing various modified nanocellulose to improve biopolymer-based films for high-barrier packaging and coating applications.

1. Introduction

Biopolymer-based film packaging has emerged as a crucial innovation in the packaging industry, addressing growing environmental concerns and consumer demand for eco-friendly alternatives.[1] This type of packaging utilizes biodegradable or compostable materials, such as plant-based polymers, to create thin, flexible films that protect products while minimizing environmental impact. These films are often derived from renewable resources, which can break down naturally in composting facilities or landfills like thermoplastic starch, polylactic acid (PLA) and cellulose derivatives.[2] Ethyl cellulose (EC) has emerged as a bio-based polymer for diverse applications in the fields of cosmetics, food and medicine. As a cellulose ether derivative, EC offers excellent film-forming capability, biocompatibility, and thermal stability.[3] More crucially, for food packaging applications, EC films do not create harmful compounds when exposed to heat. Thus, they are safe and trustworthy alternatives to plastics.[4] However, EC films have a high permeability to oxygen and a moderately high water vapor transfer rate, making them unsuitable for use in packaging films that require gas barrier properties and a prolonged shelf life.[5]

Nanofillers and nanoreinforcements integrated into biopolymers have demonstrated significant potential for reducing gas permeability in their nanocomposite films. Several nanomaterials, such as nanoclay, nanocarbon, and nanocellulose,

[a]*School of Science, Mae Fah Luang University, 333 M1, Muang, Chiang Rai, 57100, Thailand. E-mail: nattakan@mfu.ac.th*
[b]*Center of Chemical Innovation for Sustainability (CIS), Mae Fah Luang University, Chiang Rai, Thailand*
[c]*Department of Aeronautics, Imperial College London, South Kensington Campus, London, SW7 2AZ, UK*
[d]*WMG, University of Warwick, Coventry, CV4 7AL, UK*
[e]*Center of Innovative Materials for Sustainability (iMatS), Mae Fah Luang University, 333 M1, Muang, Chiang Rai, 57100, Thailand*
†Electronic supplementary information (ESI) available. See DOI: https://doi.org/10.1039/d4lp00356j

have received a lot of attention in research investigations in recent decades. Because of their distinct morphological features, different types of nanofillers exhibit varying oxygen barriers. Two-dimensional nanoclay and nanocarbon stand out due to their large aspect ratio, high specific surface area and a unique flake-like filler layered structure, which can form more tortuous molecular movement paths in a nanocomposite structure when well dispersed.[6] These nanofillers, however, have a tendency to self-agglomerate, which will hinder the enhancement of the film's barrier properties.[7–11] Nanocrystalline cellulose (NCC), a one-dimensional rigid rod-like structure, and nanofibrillated cellulose (NFC), long, thin, flexible nanofibrils with a high aspect ratio are considered excellent candidates for polymer reinforcement due to their high rigidity, strength, crystallinity and specific surface area. When they are added as a filler material into another polymer matrix, they can reduce porosity and create tortuous pathways, making gas diffusion more difficult.[12–16] Furthermore, due to its high aspect ratio, NFC can produce a twist network structure, resulting in a more tortuous diffusion path, dramatically reducing oxygen permeability.[17,18] However, there have been no reports of high barrier EC films integrated with nanocellulose or other bio-based nanofillers thus far.

NFC and NCC have been extensively studied as a reinforcing agent in bio-nanocomposite films to enhance their barrier properties. Multiple studies have demonstrated that the incorporation of nanocellulose can significantly reduce the oxygen permeability (OP) and oxygen transmission rate (OTR) in various biodegradable polymer matrices. For instance, Mondragon et al. (2015) reported that adding 5–10% NFC or NCC into a gelatin matrix decreased oxygen transmission by 21% and 36%, respectively.[19] Similarly, Kim et al. (2020) found that a self-standing film composed of succinylated NFC and a fluoropolymer exhibited a 97% reduction in oxygen transmission compared to polyethylene terephthalate (PET).[20] In another study, Kang et al. (2021) demonstrated that gum arabic films reinforced with 4% NCC showed a 25% reduction in oxygen permeability. Despite these enhancements in gas barrier performance, improving water vapor permeability (WVP) remains a greater challenge for bio-based polymer films.[21] While NFC fillers improved the WVP of PLA by 52% at 10 wt% loading, other cellulose fillers such as cocoa bean shells failed to provide WVP enhancement, even at higher loading levels.[22,23] Poly(hydroxybutylate-co-hydroxyvalerate) (PHBV)-based nanocomposites with NCC achieved a 65% decrease in OP at 2 wt%, and the incorporation of microcellulose fiber resulted in a 70% reduction in WVP at 1 wt%.[23,24] Polybutylene succinate (PBS) films reinforced with NCC and chitin whiskers also showed significant improvements (62% reduction in OP and 40% reduction in WVP at 3 wt%).[25] In the case of polycaprolactone (PCL) and polybutylate adipate terephthalate (PBAT), the addition of microcellulose fibrils or NCC also yielded moderate improvements in WVP.[26,27]

Because nanocellulose (NFC and NCC) is inherently hydrophilic, it has been shown to be difficult to considerably enhance the water vapor barrier of biopolymer films.

Furthermore, while it can be highly effective in enhancing oxygen barrier properties under dry conditions, its performance tends to diminish under high humidity. This is due to increased moisture absorption, swelling, and microstructural disruption that reduce the film's overall barrier function.[28] To address this issue, researchers have proposed various surface modifications of NFC and NCC, including acetylation, silylation, TEMPO oxidation, sulfonation, and esterification reactions.[29] Esterification is a relatively straightforward reaction that can be performed through a variety of methods, including reflux, sonication, and milling.[30] In our previous work, we used a microwave-assisted process to modify lactic acid (LA) on NFC which can reduce the esterification reaction time to only 1 min with exceptional low-energy usage.[31] The maximum degree of substitution (DS) on NFC achieved was around 0.7, and esterified NFC demonstrated enhanced dispersibility in low polarity solvents and a polylactic acid (PLA) matrix.

The insertion of long hydrophobic chains onto the surface of NFC has been shown to be one of the most effective methods for increasing its hydrophobicity. Fatty acids are abundant in the form of lipids, comprising chains of carbons and hydrogens, and contain a methyl group at one terminus and a carboxylic group at the other.[32] Saturated fatty acids like lauric acid (LU) and stearic acid (SA) have been employed as hydrophobic surface modifiers due to their low cost and high availability. LU is insoluble in water but can be dissolved in organic solvents, such as ethanol, DMSO, and dimethyl formamide, whereas the solubility of SA in ethyl acetate was determined to be the highest.[33,34] Previous investigations have never directly addressed the influence of LU and SA on the NFC surface. However, insights can be drawn from the interactions of fatty acids with other materials as compatibilizers or surface modifiers.[35] When NFC was treated with oleic acid (OA), Hadi et al.[36] reported that its surface polarity reduced, resulting in increased compatibility with the PLA matrix and improved thermal, mechanical, and water vapor barrier properties of their composite films compared to pure PLA film. Additionally, SA has been found to promote the compatibility between graphene oxide and poly(lactic acid) (PLA), enhancing the tensile properties of the composites.[37] This suggests that fatty acids appear to be very interesting choices for modifying the surface of NFC to make it more compatible with hydrophobic polymers.

In light of these considerations, the first objective of this study was to modify NFC using a microwave-assisted reaction with three esterifying agents or acids (LA, LU, and SA). Three different solvents (water, ethanol, and ethyl acetate) were utilized for NFC esterification, and their efficiency was assessed based on the DS level of the resulting modified NFC (mNFC) using titration, FTIR, XRD, SEM and dispersion behavior observation. Following NFC modification, the second objective was to study the effects of integrating these three distinct mNFCs into nanocomposite films based on the EC biopolymer. The film morphology and microstructures, mechanical and thermal properties, surface water resistance, and barrier properties of the EC-based nanocomposites were then

© 2025 The Author(s). Published by the Royal Society of Chemistry

RSC Appl. Polym., 2025, 3, 1244–1257 | 1245

investigated in order to gain insight into their potential in food packaging applications.

2.   Materials and methods

2.1.   Materials

NFC was purchased from Cellulose Lab (Canada). Ethylcellulose powder (food grade) with an ethoxyl content of 47%, and a viscosity of 50 cP was supplied by Chanjao Longevity (Myskinrecipes) Co. Ltd (Thailand). Lactic acid (LA) (90 wt%, reagent grade) and analytical grade HCl (37 wt% conc.) were purchased from Union Science (Thailand). Lauric acid 98% (LU) and stearic acid (SA) 90% powder (food/cosmetic grade) were purchased from Krungthepchemi Co. Ltd (Thailand). Analytical grade solvents (ethanol 95%, ethyl acetate 99.8%, chloroform 99.8%) were purchased from RCI Labscan (USA). All chemicals were used as received without further purification.

2.2.   Preparation of mNFC-LA, mNFC-LU and mNFC-SA in different solvent systems

In this study, mNFC was modified with three acids (LA, LU, and SA) in three solvent systems (water, ethanol, and ethyl acetate). In each solvent system, one gram of NFC was dispersed in 200 ml of solvent to prepare a NFC suspension which was homogenized (3500 rpm for 5 min) to enhance dispersion and stability, before the addition of LA, LU, or SA. Then, 0.05 M HCl was added to the system as a catalyst to increase the esterification rate. The mixture was homogenized (3500 rpm for 5 min) again before microwave heating (MS23K3513AW/ST, Samsung, Korea). The NFC : acid weight ratio was fixed at 1 : 10 and the microwave power of 800 watts and heating time of 1 min were used, based on the best conditions found in our previous study.[31] This ratio resulted in a high degree of substitution (DS) within a very short microwave-assisted esterification time and ensured an excess of the esterifying agent, promoting reaction efficiency while preventing degradation of the nanocellulose structure. During microwave irradiation, all samples were stirred using an in-house-made

polytetrafluoroethylene (PTFE) stirrer (Fig. 1) to enhance the sample's homogeneity. The final products of mNFC modified with LA, LU, and SA were labeled as mNFC-LA, mNFC-LU, and mNFC-SA, respectively, and were freeze-dried and stored in sealed plastic bags for later use.

2.3.   Preparation of EC based nanocomposite films

EC composite films were prepared with both NFC and mNFC (mNFC-LA, mNFC-LU, and mNFC-SA) at a loading concentration of 2.5 wt%. The film was prepared with a thickness in the range of 30–50 microns by solvent casting method. EC powder was dissolved in ethanol at a concentration of 5 wt% solution and mixed with NFC and each mNFC. Then, the mixture was stirred at 3500 rpm for at least 10 min and sonicated (Ultrasonic processor, VCX 750, Sonics & Materials Inc., USA) for 30 min to ensure a homogeneous dispersion without the formation of air bubbles. The mixture was later poured into the porcelain ceramic mold and dried in an oven at 60 °C for 3 h. The thickness of films was measured using ImageJ software, which analyzed SEM cross-sectional images, with thickness estimated at ten random places per film. Pure EC, EC/mNFC-LA, EC/mNFC-LU, and EC/mNFC-SA films had similar thicknesses (µm) (29.00 ± 4.85, 27.49 ± 4.47, 29.61 ± 3.43, and 28.60 ± 3.03, respectively). The greater thickness and standard deviation (±SD) found in the EC/NFC sample (41.96 ± 10.67) are likely owing to NFC aggregation in the EC matrix.

2.4.   Characterization

2.4.1.   Determining DS by the titration method. The mNFC sample (0.5 g) was stirred in 40 mL of 70% aqueous ethanol at 400 rpm for 30 min. The reaction mixture was agitated continuously for 48 hours at 50 °C after adding 20 mL of a 0.5 M NaOH solution. Subsequently, any residual unreacted NaOH was back-titrated with a 0.5 M HCl solution, and the ester content was determined using the following equation.[31]

$$EC\,(\%) = \frac{[(V_a - V_b) \times N_b - (V_d - V_c) \times N_a] \times M_w}{10 \times G} \tag{1}$$

where V_a and V_b represent the volumes (mL) of a NaOH solution added to the sample and blank, respectively. V_d and V_c
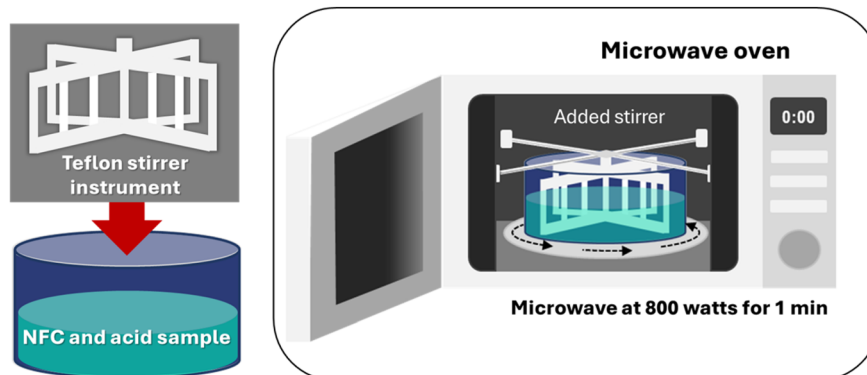

Fig. 1   Schematic of a microwave equipped with an in-house-made PTFE stirrer fixed to the internal walls.

represent the volumes (mL) of HCl added to the sample and blank, respectively. N_b and N_a stand for the concentration (in molarity) of NaOH and HCl solutions, respectively. M_w corresponds to the molecular weight of the acid reagent, while G signifies the weight (in grams) of the sample. DS was then determined by the following equation:

$$DS = \frac{162 \times EC}{M_w \times 100 - EC \times (M_w - 1)} \quad (2)$$

where 162.14 is the molecular weight of anhydroglucose monomer unit.

2.4.2. Fourier transform infrared (FTIR) spectra. The FTIR spectra of NFC and all mNFC samples were acquired utilizing a Nicolet iS50 instrument (Thermo Scientific, USA) equipped with a Universal Attenuated Total Reflectance attachment. Measurements were conducted over a range of 400 to 4000 cm^{-1}, employing a resolution of 8 cm^{-1}. Each sample underwent 32 scans to generate the resultant spectrum.

2.4.3. X-ray diffraction (XRD). The crystal structures of nanocellulose samples were analyzed using XRD (X'Pert Pro MPD, UK). Measurements were conducted over a 2θ angle range from 10° to 40°, employing a step width of 0.02° and a scanning rate of 2° min^{-1} to obtain the XRD patterns. For each sample, the crystalline index (CI) was determined using the following equation:[38]

$$CrI\,(\%) = \frac{I_{002} - I_{am}}{I_{002}} \times 100 \quad (3)$$

where I_{200} represents the peak intensity of the (200) lattice diffraction, while I_{am} denotes the intensity scattered by the amorphous portion of the sample.

2.4.4. Dispersion behavior observation. NFC and all mNFC samples in the aqueous suspension were exchanged with polar (water) and non-polar (chloroform) solvents at 0.1 wt%. The suspension was homogenized for 5 min and the results were recorded photographically at an initial time point of 5 min. Subsequently, the samples were left undisturbed for 3 weeks before being photographed again. The experiments were conducted in triplicates.

2.4.5. Nanocellulose and film morphology. The morphologies of the freeze-dried nanocellulose and film samples were examined using field emission scanning electron microscopy (FE-SEM) (TESCAN, MIRA, USA) at a 5 kV accelerating voltage. All film samples were sectioned into 5 mm × 5 mm specimens and subjected to gold coating prior to observation.

2.4.6. Water contact angle. The water contact angles of the film samples were measured with an instrument (SL200KS, KINO, Boston, MA, USA) to assess film hydrophobicity. A droplet of 5 μL water was deposited onto the film surface, and the contact angle was measured after stabilization for 15 s. All measurements were conducted at 23 °C with five replicates.

2.4.7. Thermogravimetric analysis (TGA). Thermal stability assessments of film samples were conducted using a thermogravimetric analyzer (Mettler Toledo 851e, Leicester, UK). Approximately 5 mg of each sample was weighed into an aluminum crucible and subjected to a controlled heating program from ambient temperature up to 700 °C, at a constant rate of 10 °C min^{-1}. The measurements were performed under a nitrogen atmosphere maintained at a flow rate of 50 mL min^{-1}. The acquired thermograms were used to determine the film's degradation temperature (T_d).

2.4.8. Differential scanning calorimetry (DSC) analysis. The thermal transitions of films were investigated using a differential scanning calorimeter Mettler Toledo 851e, Leicester, UK. Each sample (5 mg) was sealed in an aluminum crucible and heated from 30 °C to 300 °C at a rate of 10 °C min^{-1} under a nitrogen purge (flow rate of 50 mL min^{-1}). The glass transition temperature (T_g) and melting temperature (T_m) were determined from the recorded thermograms.

2.4.9. Tensile properties. All tensile results were obtained using a Universal Testing Machine (Instron 5566, Norwood, MA, USA). ASTM D882 was the standard used to determine the stress–strain curve, tensile strength, elongation at break, and Young's modulus. The specimen dimensions were 80 mm (L) and 15 mm (W). Five specimens were tested at a crosshead speed of 5 mm min^{-1} and a constant temperature of 23 °C, and the average values of tensile properties were calculated.

2.4.10. Water vapor transmission rate (WVTR). The WVTR of all film samples was determined following the ASTM E96/E96M standard. Circular samples, approximately 8 cm in diameter, were cut and mounted on circular aluminum cups containing 10 g of desiccant silica gel. The film samples were securely sealed to the cups using bee wax. Initial weights of the sample cups were recorded using a 4-digit analytical balance with an accuracy of 0.0001 g. The cups were then placed in a chamber maintained at 25 °C and 80% relative humidity (RH) with constant air circulation. Subsequent mass measurements were conducted until a constant weight was achieved, which indicated the amount of vapor absorbed by the desiccant. The WVTR was then determined using the following equation:

$$WVTR = \frac{W_v}{t \times A} \quad (4)$$

where W_v is the amount of water vapor (g), t is the time (days), and A is the sheet area (m^2).

2.4.11. Oxygen transmission rate (OTR). The oxygen barrier test of all film samples was conducted in accordance with ASTM D3985-02. The test results were averaged over three samples and reported as the OTR values. Tests were performed at 23 °C and 0% RH using a MOCON OX-TRAN 2/22 OTR analyzer (Minneapolis, MN, USA). Aluminum foil masks with an inner diameter of 5 cm were used to mount test pieces in the diffusion cell. In a chamber, nitrogen gas flowed across one side of a test film, which served as a membrane. On the opposite side, an oxygen stream was presented and the difference in partial pressure created a force that drives oxygen molecules to permeate through the film toward the low-pressure area. The film's oxygen permeation rate was continuously monitored and then calculated.

© 2025 The Author(s). Published by the Royal Society of Chemistry

RSC Appl. Polym., 2025, **3**, 1244–1257 | **1247**

3. Results and discussion

3.1 Modified NFC surface with lactic acid (LA), lauric acid (LU) and stearic acid (SA)

Three acids were used to modify NFC in this study. LA, with only 3 carbon atoms, easily dissolves in highly polar solvents like water. In contrast, LU and SA, which contain 12 and 18 carbon atoms respectively, have longer hydrophobic chains, making them less soluble in water. LU is soluble in alcohol, while SA is soluble in organic solvents like ethyl acetate which are less polar than water.[39] The chemical composition of each acid significantly influences its solubility in different solvents. Therefore, water, ethanol, and ethyl acetate were chosen as solvents based on the solubility characteristics of the acids. The results from the NFC esterification are presented in Table 1. LA was soluble in all solvents, and after modification, mNFC-LA exhibited varying degrees of substitution (DS) in each solvent. mNFC-LA with the lowest DS was observed in the water system, while the highest DS occurred in the ethanol system. Based on the solvatochromic properties of the solvents (Table 1), ethanol has a strong ability to both donate (α) and accept (β) protons, forming hydrogen bonds with the solute. As a result, ethanol can act as both a solvent and a reactant, increasing the kinetic constants and accelerating the esterification process.[40] In contrast, the presence of water and ethyl acetate does not necessarily impede the reaction and may even enhance it in certain conditions.[41] For NFC modification with fatty acids (LU and SA), the insolubility of acids in solvents showed a significant effect on reducing the DS of the resulting mNFCs. Both mNFC-LU and mNFC-SA showed the highest DS in the reaction with ethyl acetate. As we know, fatty acids are relatively non-polar molecules, and according to the "like dissolves like" principle, LU and SA are more soluble in non-polar solvents and less soluble in polar solvents. Solvents become less polar (π) as they progress from water and ethanol to ethyl acetate.[42,43] This indicates that the solubility of LU and SA in ethyl acetate should be the highest, hence, resulting in the highest DS of mNFC-LU and mNFC-SA in this solvent. Previous research has shown that imperatorin[44] is more soluble in ethyl acetate than in ethanol, as are salicylic acid[45]

and chlorpheniramine maleate.[46] This suggests that ethyl acetate is a more effective solvent than ethanol for dissolving non-polar substances. Indeed, increasing acid solubility increases the chemical reactivity of the reaction, thus maximizing the DS values of the present mNFCs in our investigation. It should also be noted that in ethyl acetate solvent, mNFC-LU had a higher DS than mNFC-SA, which was most likely due to the increased steric hindrance effect of the longer hydrocarbon chain of SA, which reduced chemical reactivity by physically blocking access to reactive sites or hydroxyl groups on the nanocellulose surface.[47]

To study and compare the three chemically modified cellulose nanofibers, mNFC-LA, mNFC-LU, and mNFC-SA were chosen based on their closest DS values of 0.96, 1.06, and 0.94, respectively. From Fig. 2a, all mNFC samples exhibited a carbonyl (C=O) stretch at 1738 cm^{-1}, which indicated the formation of an ester bond and confirmed successful chemical modification, as illustrated in Fig. 2b.[48,49] All samples presented similar XRD patterns with the typical peaks of cellulose I at 2θ related to the 110 and 200 reflection planes.[50] XRD spectra (Fig. 2c and d) revealed a minor decrease in the crystallinity index of mNFC-LA (70%) and mNFC-LU (64%) compared to unmodified NFC (72%). On the other hand, a great reduction in the crystallinity index after modification was observed in mNFC-SA (47%). Typically, the modification of nanocellulose with fatty acids involves attaching non-polar hydrocarbon chains onto its surface, which can disrupt the hydrogen bonding network responsible for cellulose's crystalline structure. As a result, the longer the hydrocarbon chains, the greater the disturbance in the crystal structure which led to a decrease in hydrogen bonding degree and crystallinity within the nanocellulose structure.[51–53] SEM images of all nanocellulose samples are displayed in Fig. 2e. In agreement with the XRD results, an SEM image of the freeze-dried unmodified NFC showed closely bonded and entangled nanofibrils, indicating strong hydrogen bonding interactions between them, similar to those of mNFC-LA and mNFC-LU. In contrast, mNFC-SA exhibited a significantly different morphology, with more fibrillated and divided nanofibers, which should be attributed to the longer fatty side chains causing more gaps

Table 1 Effect of solvent's solvatochromic parameters on the acid solubility and degree of substitution (DS) of modified NFC (mNFC) with fatty acids

Sample code	Acid type	Solvent	α^a	β^a	π^a	Acid-solvent solubility[b]	DS
mNFC-LA	Lactic acid (LA)	Water	1.17	0.47	1.09	+Soluble	0.77 ± 0.04
		Ethanol	0.86	0.75	0.54	+Soluble	0.96 ± 0.04
		Ethyl acetate	0.00	0.45	0.45	+Soluble	0.81 ± 0.09
mNFC-LU	Lauric acid (LU)	Water	1.17	0.47	1.09	−Insoluble	0.42 ± 0.08
		Ethanol	0.86	0.75	0.54	+Soluble	1.06 ± 0.09
		Ethyl acetate	0.00	0.45	0.45	+Soluble	1.22 ± 0.08
mNFC-SA	Stearic acid (SA)	Water	1.17	0.47	1.09	−Insoluble	0.29 ± 0.11
		Ethanol	0.86	0.75	0.54	−Insoluble	0.73 ± 0.12
		Ethyl acetate	0.00	0.45	0.45	+Soluble	0.94 ± 0.06

[a] Solvatochromic parameters for solvents; α is the hydrogen-bond donating ability, β is the hydrogen-bond accepting ability, and π is the polarisability/polarity.[42,43] [b] Solubility of acids in solvents observed at room temperature (23 °C).
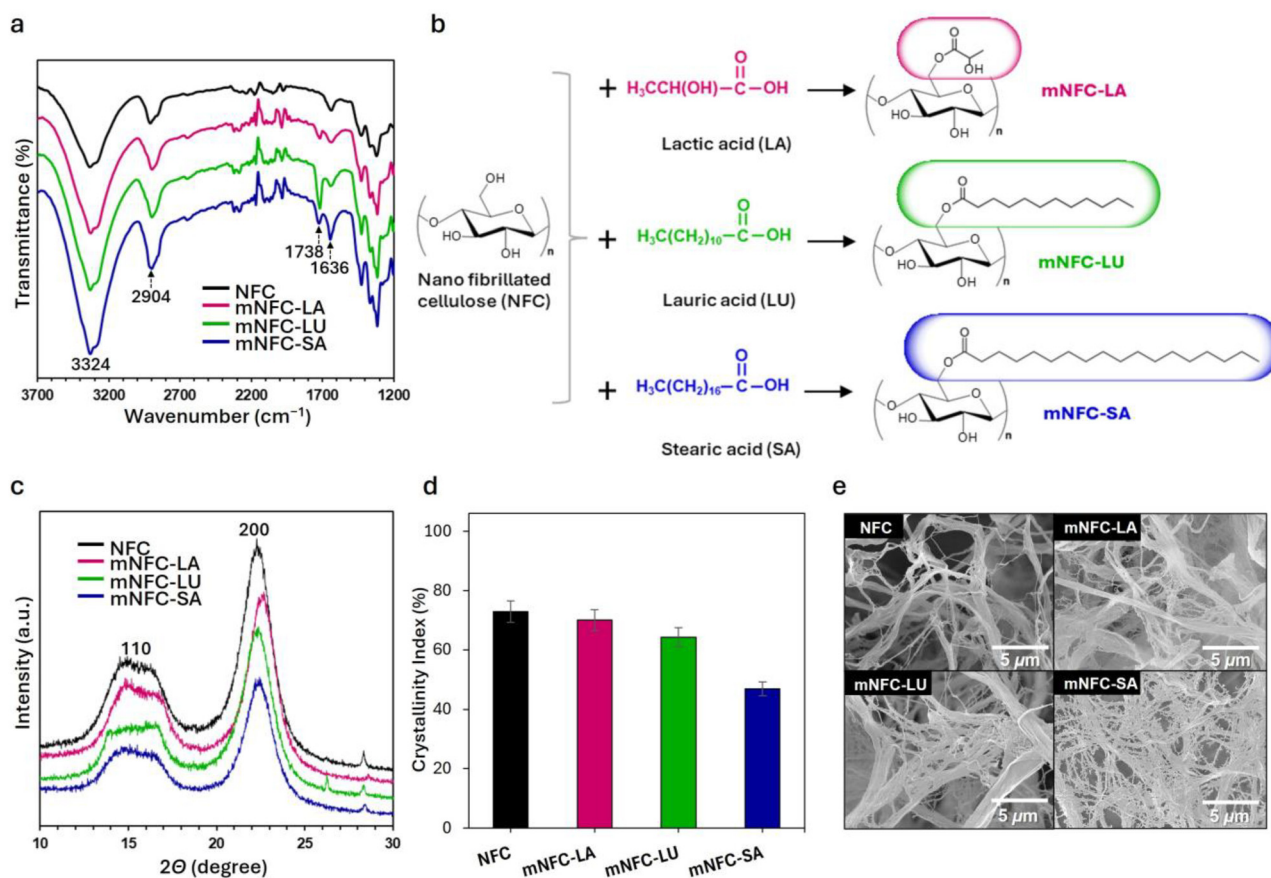
Fig. 2 (a) FTIR spectra; (b) idealized reaction scheme representation of NFC esterification with LA, LU, and SA; (c) XRD spectra; (d) crystallinity index and (e) SEM images of unmodified NFC and modified NFC (mNFC-LA, mNFC-LU and mNFC-SA).

and disturbance between cellulosic backbones and its crystalline structure.

The photographs of NFC and mNFC dispersions in different solvents are shown in Fig. 3. Initially (after homogenizing and 5 min rest), all nanocellulose samples dispersed rather well in water (polar solvent) due to the hydrophilic nature of cellulose and their nanosize, with a large surface area and extensive hydroxyl groups available on the surface. However, after 3 weeks, these nanocellulose suspensions sedimented at different levels in the following order: NFC < mNFC-LA–mNFC-LU < mNFC-SA. The unmodified hydrophilic NFC was more stable in water than the modified ones as expected. Longer side chains on mNFC should increase its hydrophobicity and sedimentation in water.[54] However, both mNFC-LA and mNFC-LU showed identical levels of sedimentation. One possibility is that the DS of mNFC-LU (1.06) was somewhat greater than that of mNFC-LA (0.96). Significant nanofiber sedimentation was noted in the mNFC-SA suspension. When the nanocellulose samples were dispersed in chloroform (non-polar solvent), NFC showed poor dispersion after 5 min, whereas all mNFC samples demonstrated an initially stable dispersion. This could be attributed to the presence of ester groups on the surfaces of these mNFC samples. After a period of 3 weeks, there was still no sedimentation in

any of the mNFC samples, demonstrating that the non-polar hydrocarbon side chains of fatty acid on the mNFC surfaces can efficiently facilitate a well-suspended and dispersed mNFC in the non-polar solvent.[55] This also highlighted that all mNFC types should be more compatible with non-polar or hydrophobic polymer matrices and able to make more efficient composite materials.

3.2 Effect of an mNFC substituted side chain on EC/nanocellulose composite films

The focus of this section is to compare the dispersion behavior of the three mNFC samples, each modified with a different acid, within the EC matrix, and to evaluate their influence on the structure and properties of the resulting nanocomposite films. Representative images of pure EC solution (EC), EC solution mixed with NFC (EC/NFC), and EC solution mixed with mNFC (EC/mNFC) and their casted films are provided in the ESI.† Pure EC is more transparent than other samples, in both solution and film forms. It is evident that only the integration of unmodified NFC into EC resulted in visible white spots of NFC agglomerations, potentially attributed to the strong hydrogen bonding network and van der Waals forces between NFC nanofibers themselves.[56] From visual inspection, no mNFC agglomeration was observed in any of the EC/mNFC samples,

© 2025 The Author(s). Published by the Royal Society of Chemistry

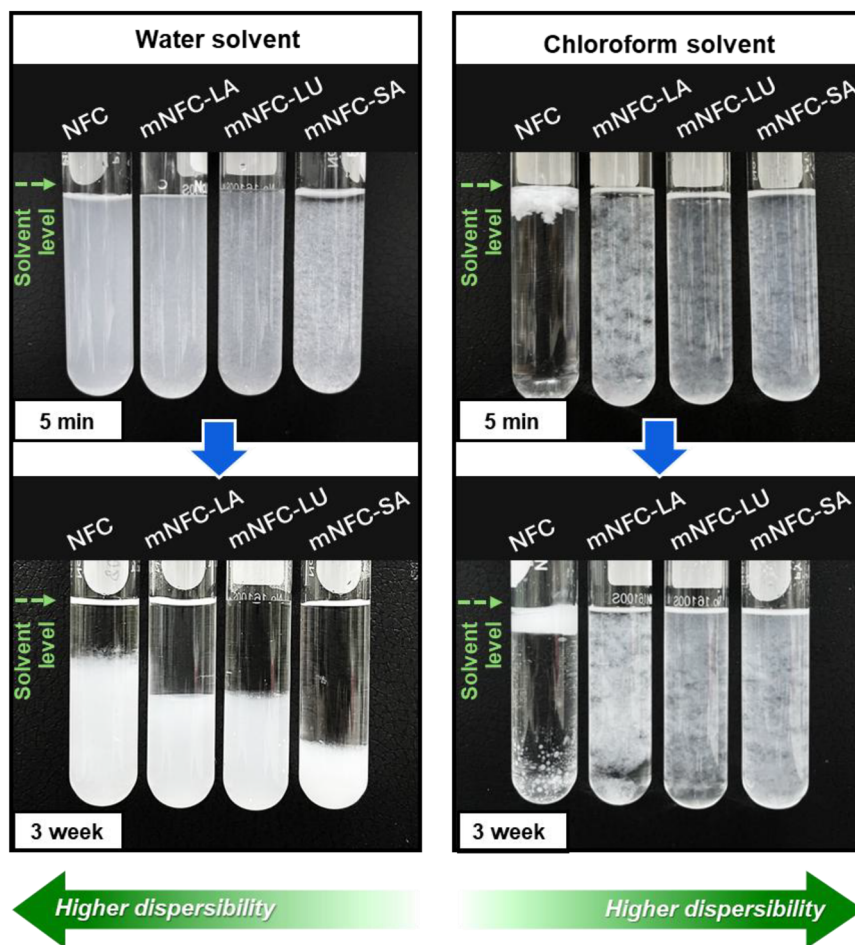*RSC Appl. Polym.*, 2025, **3**, 1244–1257 | **1249**

Fig. 3 Dispersion behavior in a polar solvent (water) and a non-polar solvent (chloroform) at 5 min and after 3 weeks of unmodified and modified NFC with different acids (mNFC–L+A, mNFC–LU and mNFC–SA).

indicating that mNFC and EC were more compatible in both solution and film samples.

Water contact angle (WCA) measurements are used to determine the hydrophilicity and hydrophobicity of polymer film surfaces, with higher WCA values indicating more hydrophobicity. Pure EC film had a WCA of 64° (Fig. 4a), demonstrating its amphiphilic character, as the glucopyranoside structure in EC associates both hydrophilicity and hydrophobic interactions.[57] The EC/NFC film exhibited a lower WCA of 55°, owing to the strong hydrophilicity of the integrated NFC and its agglomeration on the film surface.[58] When mNFCs were included in EC films, WCA values increased in the following order: EC/mNFC-SA > EC/mNFC-LU > EC-mNFC-LA. Undoubtedly, this increase in hydrophobicity was due to the presence of hydrophobic side chains on mNFC surfaces. As expected, longer hydrocarbon chains in SA and LU resulted in much greater WCA of the EC/mNFC-SA and EC/mNFC-LU films.

From SEM results (Fig. 4b), the EC film exhibited a uniform and smooth surface. The introduction of NFC resulted in a rougher film surface, most likely due to NFC agglomeration (indicated with red circles). The EC/mNFC-LA and EC/

mNFC-LU films showed smoother surfaces than the EC/NFC film, indicating that less nanofiber agglomeration occurred in these films. However, the surface roughness was found to increase again in the EC/mNFC-SA film. This roughness could be attributed to the long hydrophobic side chains of SA fatty acid, which caused mNFC-SA to require more free volume or space to occupy (compared to the other two mNFCs; Fig. 5) within the EC matrix. This potentially led the film surface to be less homogeneous and rougher.[59,60] SEM images of the EC-based films' fractured surface (cross-section) are shown in Fig. 4c. The pure EC film displayed numerous visible pores inside. NFC agglomerates in the EC phase can also be easily seen when unmodified NFC is added (indicated with red circles). However, these agglomerates were not found in the EC films integrated with any of the mNFCs. Furthermore, the pores inside these EC/mNFC films appear to be smaller than those in the pure EC film.

TGA and DTG thermograms of films are depicted in Fig. 6a and b. The first (small) weight loss stage occurred around 50–100 °C for all film samples, attributed to the evaporation of free water. The second weight loss stage, occurring between 300 °C and 380 °C, represented the main degradation phase,
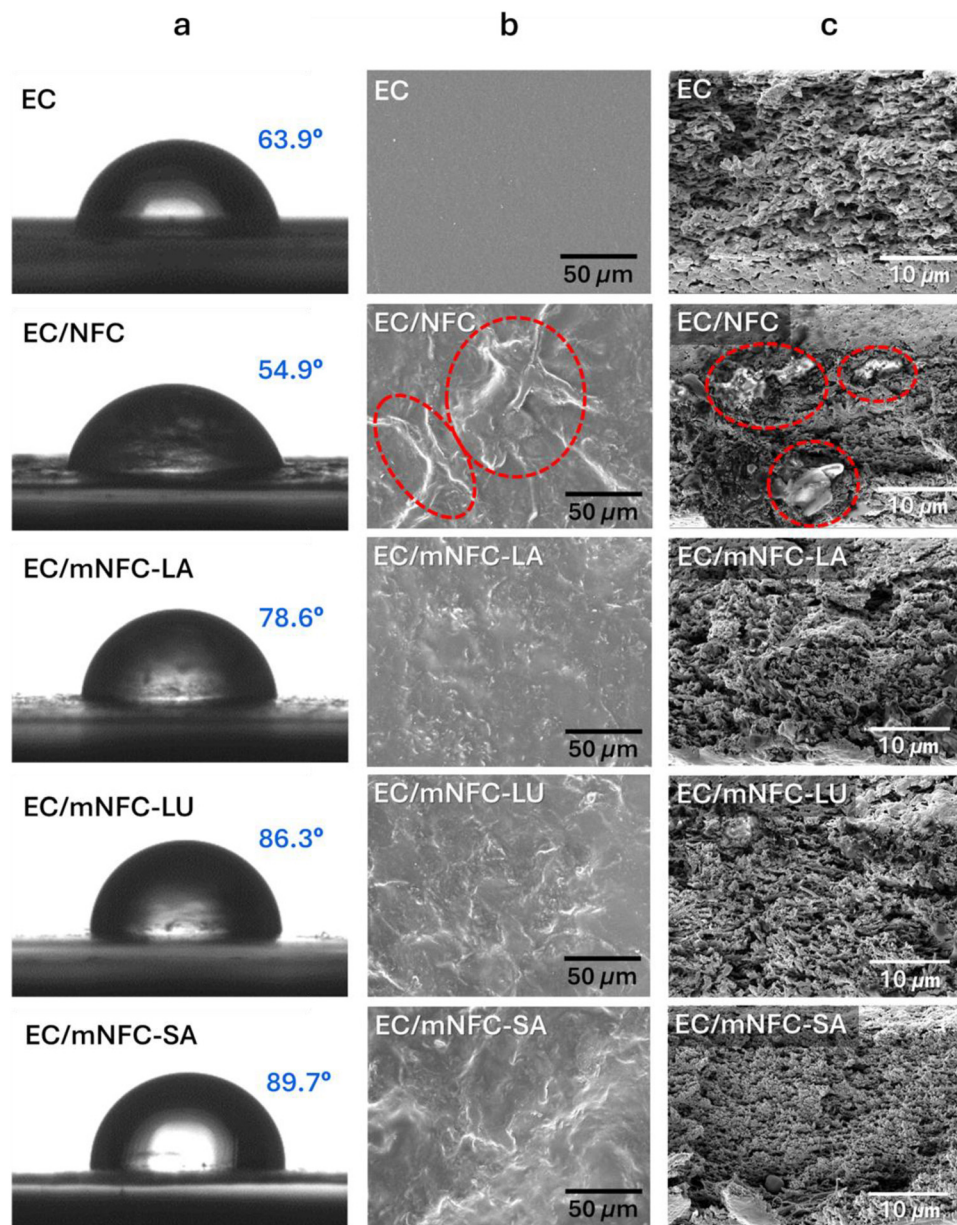
Fig. 4 (a) Water contact angle (WCA) or surface wettability, (b) SEM images of pure EC and EC-based nanocomposite film surfaces and (c) their cross-sections (fractured surfaces); the red circles indicate NFC agglomerates.

involving the degradation of EC, NFC and mNFC, with around 10–20% of char generated after this stage. The maximum degradation temperature (T_d) of each film is shown in Table 2. The T_d values of EC/mNFC films were observed to be higher than the pure EC and EC/NFC films, implying that the ester group on mNFC is more thermally stable and that EC and mNFC interact better.[61,62] The DSC thermograms (Fig. 6c) presented that upon the addition of NFC to the EC matrix, an increase in T_g and T_m was observed. This elevation can be attributed to the restricted mobility of the EC polymer chains, resulting from the presence of more rigid NFC agglomerates, thereby requiring more thermal energy to initiate chain segmental motion. Interestingly, all EC/mNFC-containing films show a shift in T_g and T_m to lower temperatures rather than an increase, especially the EC/mNFC-SA film (Table 2). Unlike NFC, better dispersed surface-modified nanocelluloses may act as modest internal plasticizers, leading to higher chain mobility. With the presence of esterified side chains, particularly those with longer alkyl chains, it may increase free volume and disrupt the tight packing of EC molecules at higher temperatures.[63]

The tensile strength, elongation at break, and Young's modulus of EC, EC/NFC, and EC/mNFC nanocomposite films are listed in Table 2. The EC/NFC film has lower strength and modulus than the pure EC film, most likely due to poor film compatibility and the presence of NFC agglomerates, which
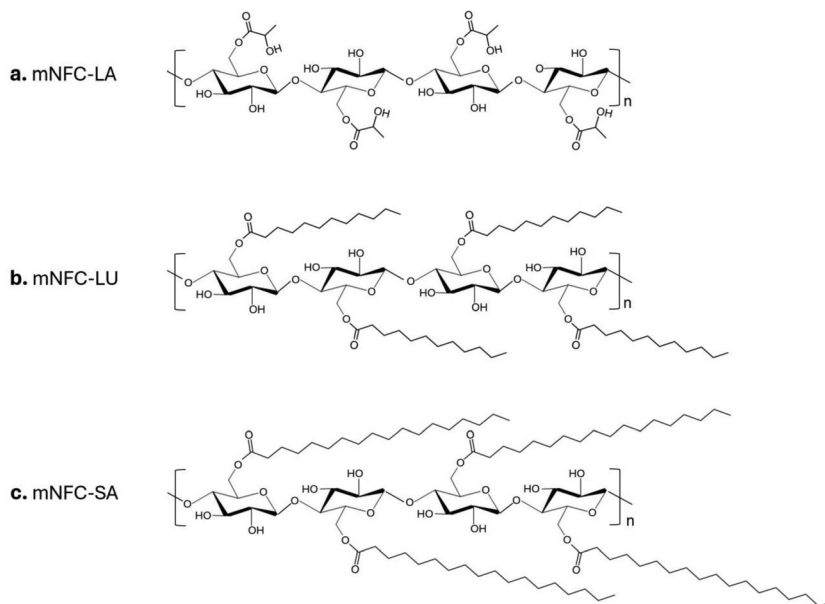
© 2025 The Author(s). Published by the Royal Society of Chemistry

RSC Appl. Polym., 2025, **3**, 1244–1257 | **1251**

Fig. 5 Schematic representation of the ideal chemical structures of the modified nanocelluloses (mNFC) with three acids/esterifying agents: (a) lactic acid (LA), (b) lauric acid (LU) and (c) stearic acid (SA).

might act as flaws and crack initiation points (Fig. 5). Remarkably, the tensile properties of the mNFC-LA film were all improved, particularly its strength (128% increase) and elongation (75% increase). This result could be explained by the increased dispersibility of mNFC-LA within the EC matrix. It also indicated a favorable interfacial interaction between the mNFC-LA and EC polymer chains.[64] The stress–strain curves in Fig. 6d also reveal that the EC/mNFC-LA film (pink line) exhibited greater toughness (represented by the area under the curve) and stiffness (slope of the curve). This is visually confirmed by the top-right image, in which the film looks to be self-supporting, emphasizing its increased structural integrity.[65] However, with mNFC-LU and mNFC-SA, with longer side chain fatty acids, the tensile properties of these EC-based films started to drop unexpectedly. Considering their chemical structures (see Fig. 5), it is possible that longer substituted chains on mNFC resulted in an excessive plasticizing effect, which weakens the interfacial adhesion between EC chains and mNFC-LU or mNFC-SA.[66] This would certainly lessen the reinforcing effect of the mNFCs as well as the cohesive forces within the EC polymer network, resulting in overall lower mechanical properties for these nanocomposite films.[67]

The films' gas barrier properties (OTR and WVTR) showed rather consistent patterns with their mechanical properties (Table 2). As expected, the structure of EC with numerous pores inside permits oxygen and water molecules to flow through quite easily. The integration of NFC negatively resulted in very high OTR and almost doubled the WVTR value of the film due to its agglomeration and poor interface with the EC matrix. These resulted in the formation of microvoids and interfacial gaps, which reduced matrix continuity and facilitated gas and vapor diffusion, as previously reported.[68] At

equivalent nanocellulose concentrations, on the other hand, the EC/mNFC-LA film had impressively low OTR and WVTR, implying a good dispersion of mNFC-LA with a high compatibility and a strong interface with the EC phase. From a diffusion modeling perspective, the addition of mNFC-LA appears to reduce gas permeability by creating a more tortuous path and minimizing free volume at the polymer–filler interface. The highly compatible interface most likely reduces the number of microvoids and forms a denser, more continuous phase, making it more difficult for gas molecules to diffuse through the film.[69,70] The EC/mNFC-LU and EC/mNFC-SA films, however, demonstrated increasing OTR and WVTR values when mNFC substituted side chains were longer. An excessive plasticizing effect may be the cause of weaker interfacial connection between these modified cellulose nanofibers and EC matrix, resulting in greater free volume at the interface and gaps inside these nanocomposite films, hence, less obstructed paths for gas molecules to permeate through.[71] These observations support the hypothesis that the gas and vapor transport mechanisms in nanocomposites are governed not only by filler dispersion and concentration but also by the extent of interfacial adhesion and microstructural continuity. A significant decrease in crystallinity following mNFC-LU and mNFC-SA modification could be another cause for the lower barrier properties in these EC-based films.

Fig. 7a compares the OTR reduction (%) of our work films with other previous bio-based nanocomposite films combined with nanofillers in the groups of polysaccharide, graphene, and clay.[72–79] As the oxygen transmission rate (OTR) is highly dependent on film thickness, and thus, direct comparison across films of varying thicknesses must be interpreted cautiously. Our current EC-based nanocomposite films had a
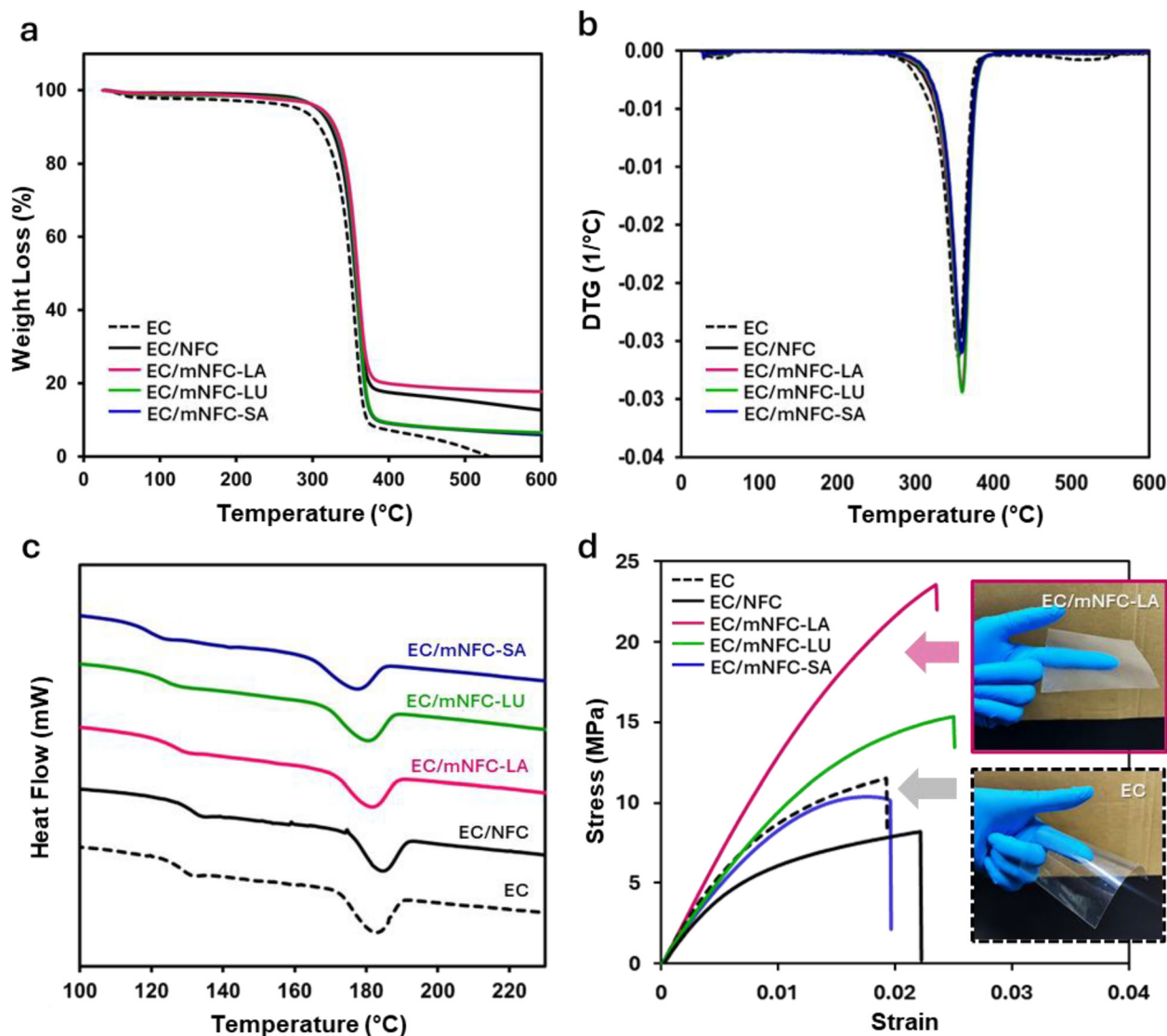
1252 | *RSC Appl. Polym.*, 2025, **3**, 1244–1257

© 2025 The Author(s). Published by the Royal Society of Chemistry

Fig. 6 (a) Thermogravimetric analysis (TGA); (b) derivative thermogravimetric (DTG) curves; (c) differential scanning calorimetry (DSC) thermograms; and (d) representative stress–strain curves of films. Insets show a visual self-standing comparison of the EC and EC/mNFC-LA films.

Table 2 Thermal, mechanical and barrier properties of the EC-based films

Properties	EC	EC/NFC	EC/mNFC-LA	EC/mNFC-LU	EC/mNFC-SA
T_d (°C)	355	357	359	360	360
T_g (°C)	131	134	129	128	123
T_m (°C)	182	184	181	180	177
σ (MPa)	10.1 (1.2)	7.4 (0.8)	23.2 (0.8)	15.4 (2.6)	10.7 (0.4)
ε (%)	1.6 (0.3)	1.8 (0.4)	2.8 (0.4)	2.3 (0.6)	1.7 (0.1)
E (GPa)	1.33 (0.017)	1.02 (0.017)	1.45 (0.067)	1.10 (0.042)	1.15 (0.012)
OTR (cc m^{-2} day^{-1})	6478 (1971)	34 235 (4381)	137 (24)	408 (128)	1575 (546)
WVTR (g m^{-2} day^{-1})	250 (43)	422 (86)	31 (20)	50 (16)	145 (35)

T_d represents the peak degradation temperatures in DTG curves, T_g (glass transition temperatures) and T_m (melting temperatures) were obtained from the DSC analysis, σ refers to the tensile strength, E refers to the Young's modulus, ε refers to the elongation at break, OTR refers to the oxygen transmission rate and WVTR refers to the water vapor transmission rate.

similar thickness of 27–30 μm. Most films reported in the literature ranged in thickness from 45–100 μm. The graph, however, reveals that the EC/mNFC-LA film presented herein has the greatest potential for reducing OTR (98% reduction) among nanocomposite films, even at a modest NFC content of 2.5 wt% and substantially lower film thickness. In addition, unlike other bio-based nanocomposite films, the EC/mNFC-LA film developed in this study has significantly improved barrier properties for both OTR and WVTR values, allowing the EC film to be upgraded to PET film properties (Fig. 7b). Thus, the mNFC-LA addition enables the EC film to be effectively utilized as an eco-friendly alternative to PET film. The use of bio-based and biodegradable films rather than petroleum-based

films can contribute to lowering the overall carbon footprint during the life cycle of a packaging material from raw material extraction to disposal, aligning with worldwide initiatives toward net-zero emissions, climate mitigation, and sustainable development.[96]

4. Conclusions

In conclusion, this study demonstrates the successful modification of nanofibrillated cellulose (NFC) using three acids/esterifying agents with different carbon chain lengths, as well as the effective integration of modified NFC (mNFC) into ethyl
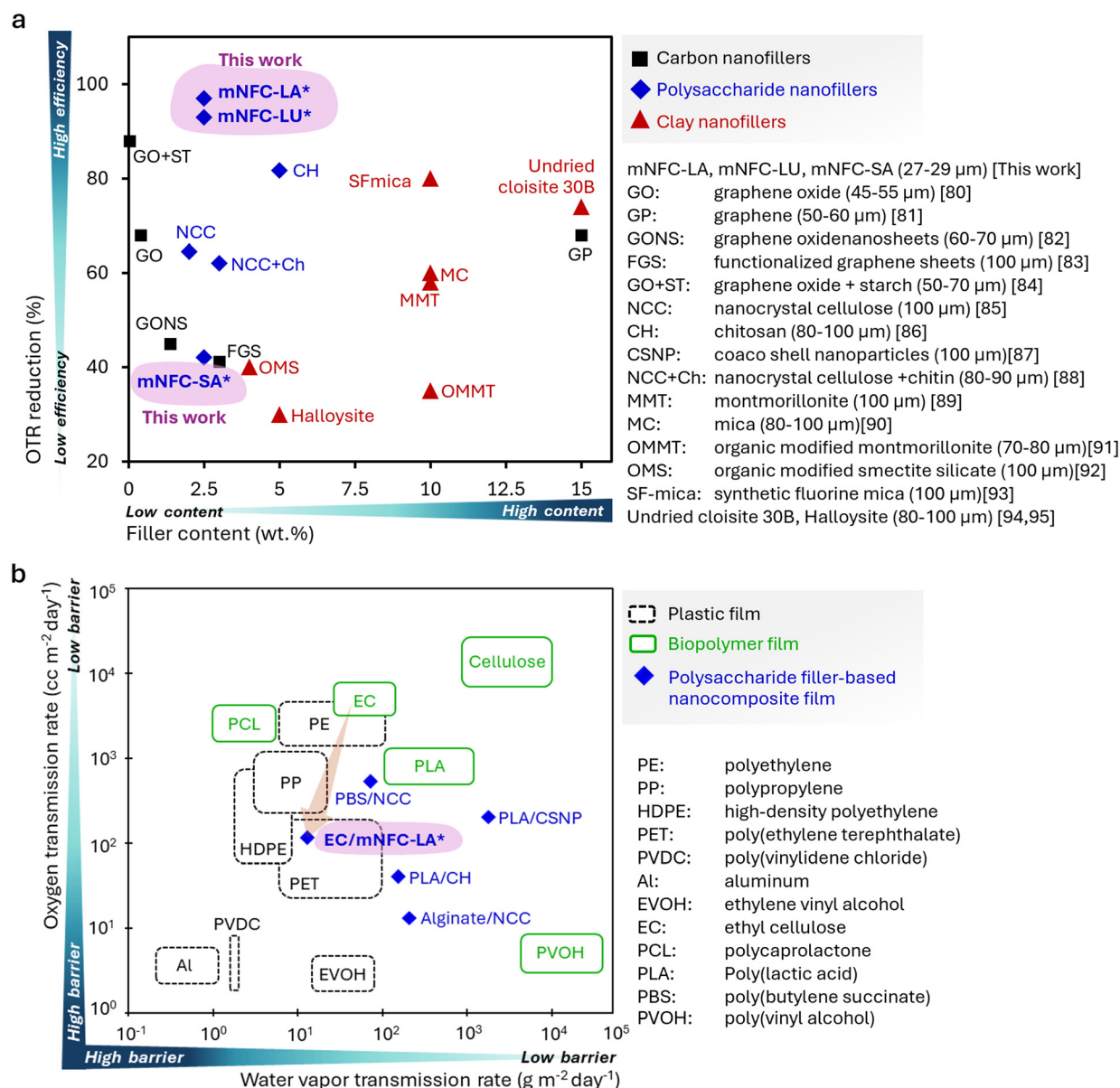

Fig. 7 (a) Comparison of OTR reduction in bio-nanocomposite films combined with nanofillers in the groups of polysaccharide, graphene, and clay. The film thickness and reference(s) are in the brackets (–) and [–], respectively; (b) OTR and WVTR of conventional packaging films and the current EC-based nanocomposite films.[80–95]

1254 | *RSC Appl. Polym.*, 2025, **3**, 1244–1257

© 2025 The Author(s). Published by the Royal Society of Chemistry

cellulose (EC) films, to improve its mechanical and barrier properties. Lactic acid (LA), lauric acid (LU), and stearic acid (SA) were used as modifying agents for NFC's microwave-assisted esterification, with a resulting degree of substitution (0.29–1.22) influenced by the solvent used (water, ethanol, and ethyl acetate). mNFC-LA exhibited the least disruption in its cellulose's crystalline structure, while mNFC-LU and mNFC-SA showed greater reductions in crystallinity due to their longer hydrocarbon side chains. All mNFC types demonstrated improved dispersion in non-polar solvents compared to unmodified NFC, suggesting enhanced compatibility with hydrophobic matrices. It was found that mNFC had no significant effect on the thermal properties of EC films. Among the EC films containing mNFC, EC/mNFC-LA showed superior tensile properties compared to the EC/mNFC-LU and EC/mNFC-SA films. Furthermore, the EC/mNFC-LA film showed a significant reduction in the oxygen transmission rate (OTR) and the water vapor transmission rate (WVTR) comparable to the values of plastic films such as PET. The findings of this study highlight the potential of mNFC, particularly mNFC-LA, as a highly effective reinforcement for enhancing the properties of bio-based ethyl cellulose (EC) films. The increased performance of the current bio-nanocomposite film bodes well for applications in sustainable food packaging, providing a viable alternative to traditional plastic films while addressing environmental concerns and meeting consumer demand for eco-friendly packaging solutions. In the future, the environmental sustainability indexes such as the carbon footprint and life cycle assessment (LCA) of these films should be evaluated, especially as food packaging materials.

Data availability

The data supporting this article are available from the authors on reasonable request.

Conflicts of interest

There are no conflicts of interest to declare.

Acknowledgements

References

1 U. Amin, M. U. Khan, Y. Majeed, M. Rebezov, M. Khayrullin, E. Bobkova and M. Thiruvengadam, *Int. J. Biol. Macromol.*, 2021, **183**, 2184–2198.

2 K. Dhali, M. Ghasemlou, F. Daver, P. Cass and B. Adhikari, *Sci. Total Environ.*, 2021, **775**, 145871.

3 A. R. Rajabi-Siahboomi, R. Y. Mehta, V. Ambudkar, V. Dias and S. Tiwari, in *Multiparticulate Drug Delivery: Formulation, Processing and Manufacturing*, 2017, pp. 267–299.

4 X. Su, Z. Yang, K. B. Tan, J. Chen, J. Huang and Q. Li, *Carbohydr. Polym.*, 2020, **241**, 116259.

5 E. Shlush and M. Davidovich-Pinhas, *Food Packag. Shelf Life*, 2023, **40**, 101206.

6 W. Han, J. R. Chen, D. Q. Wang, K. M. Mccreary, H. Wen, A. G. Swartz, *et al.*, *Nano Lett.*, 2012, **12**(7), 3443–3447.

7 C. S. Heon, C. M. Suk, L. D. Hyun and J.-D. Na, *Polymers*, 2005, **29**(4), 399–402.

8 Q. Zhang, C. An, S. Fan, S. Shi, R. Zhang, J. Zhang, *et al.*, *Nanotechnology*, 2018, **29**(28), 285501.

9 K. K. Khichar, S. B. Dangi, V. Dhayal, U. Kumar, S. Z. Hashmi, V. Sadhu, *et al.*, *Polym. Compos.*, 2020, **41**(7), 2792–2802.

10 O. V. Alekseeva, A. V. Noskov and A. V. Agafonov, *Cellulose*, 2022, **29**(7), 3947–3961.

11 M. E. Reyes-Melo, I. Y. Miranda-Valdez, J. G. Puente-Córdova, C. A. Camarillo-Hernández and B. López-Walle, *Cellulose*, 2021, **28**, 9227–9240.

12 W. L. Zhang, Y. Q. Zhang, J. K. Cao and W. B. Jiang, *Int. J. Biol. Macromol.*, 2021, **166**, 288–296.

13 B. Mekuye and B. Abera, *Nano Sel.*, 2023, **4**(8), 486–501.

14 N. Lavoine, I. Desloges, A. Dufresne and J. Bras, *Carbohydr. Polym.*, 2012, **90**(2), 735–764.

15 A. B. Perumal, R. B. Nambiar, J. A. Moses and C. Anandharamakrishnan, *Food Hydrocolloids*, 2022, **127**, 107484.

16 F. G. Hu, J. S. Zeng, Z. Cheng, X. J. Wang, B. Wang, Z. T. Zeng, *et al.*, *Carbohydr. Polym.*, 2021, **254**(8), 117474.

17 L. Wang, C. Chen, J. Wang, D. J. Gardner and M. Tajvidi, *Food Packag. Shelf Life*, 2020, **23**, 100464.

18 Y. Xu, Z. Wu, A. Li, N. Chen, J. Rao and Q. Zeng, *Polymers*, 2024, **16**(3), 423.

19 G. Mondragon, C. Peña-Rodriguez, A. González, A. Eceiza and A. Arbelaiz, *Eur. Polym. J.*, 2015, **62**, 1–9.

20 J.-K. Kim, B. Choi and J. Jin, *Carbohydr. Polym.*, 2020, **249**, 116823.

21 S. Kang, Y. Xiao, X. Guo, A. Huang and H. Xu, *Food Chem.*, 2021, **350**, 129199.

22 S. S. Nair, H. Chen, Y. Peng, Y. Huang and N. Yan, *ACS Sustainable Chem. Eng.*, 2018, **6**(8), 10058–10068.

23 E. L. Papadopoulou, U. C. Paul, T. N. Tran, G. Suarato, L. Ceseracciu, S. Marras and A. Athanassiou, *ACS Appl. Mater. Interfaces*, 2019, **11**(34), 31317–31327.

24 P. Dhar, U. Bhardwaj, A. Kumar and V. Katiyar, *Polym. Eng. Sci.*, 2015, **55**(10), 2388–2395.

© 2025 The Author(s). Published by the Royal Society of Chemistry

RSC Appl. Polym., 2025, **3**, 1244–1257 | **1255**

25 J. Xu, P. H. Manepalli, L. Zhu, S. Narayan-Sarathy and S. Alavi, *J. Polym. Res.*, 2019, **26**, 1–10.

26 M. D. Sanchez-Garcia, E. Gimenez and J. M. Lagaron, *Carbohydr. Polym.*, 2008, **71**(2), 235–244.

27 C. L. Morelli, N. Belgacem, R. E. Bretas and J. Bras, *J. Appl. Polym. Sci.*, 2016, **133**(34), 43678.

28 M. Maturi, C. Spanu, N. Fernández-Delgado, S. I. Molina, M. C. Franchini, E. Locatelli and A. S. de León, *Addit. Manuf.*, 2023, **61**, 103342.

29 H. Liimatainen, J. Sirviö, M. Visanko, O. Hormi and J. Niinimäki, *Cellulose*, 2013, **20**, 741–749.

30 M. Ghasemlou, F. Daver, E. P. Ivanova, Y. Habibi and B. Adhikari, *Prog. Polym. Sci.*, 2021, **119**, 101418.

31 S. Klayya, P. Pripdeevech, H. Zhang, E. Bilotti and N. Soykeabkaew, *Nanocomposites*, 2023, **9**(1), 171–182.

32 B. M. Trinh and T. Mekonnen, *Polymer*, 2018, **155**, 64–74.

33 C. W. Jeon, S. Park, J. H. Bang, S. Chae, K. Song and S. W. Lee, *Coatings*, 2018, **8**(1), 43.

34 R. Heryanto, M. Hasan, E. C. Abdullah and A. C. Kumoro, *ScienceAsia*, 2007, **33**, 469–472.

35 J. D. Rusmirović, M. P. Rančić, V. B. Pavlović, V. M. Rakić, S. Stevanović, J. Djonlagić and A. D. Marinković, *Macromol. Mater. Eng.*, 2018, **303**(8), 1700648.

36 H. Almasi, A. K. Asl, A. A. Entezami, J. Dehghannya and B. Ghanbarzadeh, *Food Packag. Shelf Life*, 2015, **5**, 21–31.

37 W. Chartarrayawadee, R. Molloy, A. Ratchawet, N. Janmee, M. Butsamran and K. Panpai, *Polym. Compos.*, 2017, **38**(10), 2272–2282.

38 L. Segal, J. J. Creely, A. E. Martin Jr and C. M. Conrad, *Text. Res. J.*, 1959, **29**(10), 786–794.

39 S. Gogoi, S. Hazarika, P. G. Rao and N. N. Dutta, *Biocatal. Biotransform.*, 2006, **24**(5), 343–351.

40 S. Baco, M. Klinksiek, R. I. B. Zakaria, E. A. Garcia-Hernandez, M. Mignot, J. Legros, *et al.*, *Chem. Eng. Sci.*, 2022, **260**, 117928.

41 A. Jouyban and E. Rahimpour, *J. Iran. Chem. Soc.*, 2022, **19**(1), 1–22.

42 M. Peña-Fernández, G. Spanò, N. S. Torres-Pabón and F. Martínez, *Ars Pharm.*, 2023, **64**(4), 329–324.

43 A. Alimmari, B. Božić, D. Mijin, A. Marinković, N. Valentić and G. Ušćumlić, *Arabian J. Chem.*, 2015, **8**(2), 269–278.

44 X. Zhang, Y. Xie, W. Cao, Q. Yang, S. Miao and S. Wang, *Chromatographia*, 2011, **74**, 259–265.

45 A. Shalmashi and A. Eliassi, *J. Chem. Eng. Data*, 2008, **53**(1), 199–200.

46 Q. S. Li, Y. M. Tian and S. Wang, *J. Chem. Eng. Data*, 2007, **52**(6), 2163–2165.

47 X. Wang, N. Wang, B. Xu, Y. Wang, J. Lang, J. Lu, *et al.*, *Polymers*, 2021, **13**(19), 3417.

48 G. A. G. Giraldo, J. Mantovan, B. M. Marim, J. O. F. Kishima and S. Mali, *Polysaccharides*, 2021, **2**(2), 218–233.

49 T. Widjaja, N. Hendrianie, S. Nurkhamidah, A. Altway, B. Yusuf, F. Fakhrizal, *et al.*, *Heliyon*, 2023, **9**(8), 17985.

50 J. F. Pedrosa, M. G. Rasteiro, C. P. Neto and P. J. Ferreira, *Int. J. Biol. Macromol.*, 2022, **201**, 468–479.

51 C. Liu, B. Li, H. Du, D. Lv, Y. Zhang, G. Yu, *et al.*, *Carbohydr. Polym.*, 2016, **151**, 716–724.

52 L. Duchatel-Crépy, N. Joly, P. Martin, A. Marin, J. F. Tahon, J. M. Lefebvre and V. Gaucher, *Carbohydr. Polym.*, 2020, **234**, 115912.

53 S. Klayya, N. Tawichai, U. Intatha, H. Zhang, E. Bilotti and N. Soykeabkaew, *Nanocomposites*, 2021, **7**(1), 109–122.

54 X. Guo, Y. Wu and X. Xie, *Sci. Rep.*, 2017, **7**(1), 14207.

55 Y. Zhao, W. Dang, Q. Ma and Y. Zhu, *Cellulose*, 2019, **26**, 4345–4355.

56 A. M. Mahmoud, J. P. Morrow, D. Pizzi, A. M. Azizah, T. P. Davis, R. F. Tabor and K. Kempe, *Biomacromolecules*, 2020, **21**(8), 3007–3016.

57 L. Alves, B. F. Medronho, F. E. Antunes, A. Romano, M. G. Miguel and B. Lindman, *Colloids Surf., A*, 2015, **483**, 257–263.

58 Y. Lin, F. O. Asante, X. Xu, S. Li, H. Ding, L. Xu, *et al.*, *Cellulose*, 2021, **28**, 289–300.

59 I. Elfaleh, F. Abbassi, M. Habibi, F. Ahmad, M. Guedri, M. Nasri and C. Garnier, *Results Eng.*, 2023, 101271.

60 I. Tagliaro, M. Mariani, R. Akbari, M. Contardi, M. Summa, F. Saliu, *et al.*, *Carbohydr. Polym.*, 2024, **333**, 121981.

61 M. L. Li, D. F. Hou, P. Y. Li, Z. W. Feng, Y. H. Huang, F. Wang and M. B. Yang, *ACS Sustainable Chem. Eng.*, 2024, **12**(26), 9669–9681.

62 Y. Zhou, Y. Hu, Z. Tan and T. Zhou, *J. Cleaner Prod*, 2024, **439**, 140839.

63 B. Liu, F. Sun, P. Zhu, K. Wang, L. Peng, Y. Zhuang and H. Li, *Int. J. Biol. Macromol.*, 2024, **278**, 134557.

64 L. Huang, X. Zhang, M. Xu, J. Chen, Y. Shi and C. Huang, *AIP Adv.*, 2018, **8**(2), 025116.

65 C. J. Chirayil, J. Joy, L. Mathew, J. Koetz and S. Thomas, *Ind. Crops Prod.*, 2014, **56**, 246–254.

66 N. Ratsameetammajak, R. Molloy and R. Somsunan, *Plast., Rubber Compos.*, 2018, **47**(4), 139–146.

67 X. Li, S. Luo, Y. Hou, Y. Liu, X. Hu and C. Liu, *Int. J. Biol. Macromol.*, 2020, **155**, 1069–1074.

68 V. Siracusa, *Int. J. Polym. Sci.*, 2012, **2012**(1), 302029.

69 L. Meng, S. Li, W. Yang, R. Simons, L. Yu, H. Liu and L. Chen, *ACS Sustainable Chem. Eng.*, 2019, **7**(10), 9506–9514.

70 S. Klayya, N. Tawichai, U. Intatha, H. Zhang, E. Bilotti and N. Soykeabkaew, *Polym. Int.*, 2023, **72**(3), 323–332.

71 H. Faraj, N. Follain, C. Sollogoub, G. Almeida, C. Chappey and S. Marais, *Polym. Test.*, 2022, **113**, 107683.

72 J. W. Rhim and P. K. Ng, *Crit. Rev. Food Sci. Nutr.*, 2007, **47**(4), 411–433.

73 A. Saxena, T. J. Elder, J. Kenvin and A. J. Ragauskas, *Nano-Micro Lett.*, 2010, **2**, 235–241.

74 E. Fortunati, M. Peltzer, I. Armentano, A. Jiménez and J. M. Kenny, *J. Food Eng.*, 2013, **118**(1), 117–124.

75 R. Shanmugam, V. Mayakrishnan, R. Kesavan, K. Shanmugam, S. Veeramani and R. Ilangovan, *J. Polym. Environ.*, 2022, **30**(5), 1749–1757.

76 I. U. Unalan, D. Boyacı, M. Ghaani, S. Trabattoni and S. Farris, *Nanomaterials*, 2016, **6**(12), 244.

77 D. B. Lee, D. W. Kim, Y. Shchipunov and C. S. Ha, *Polym. Int.*, 2016, **65**(9), 1039–1045.

78 R. Cosquer, S. Pruvost and F. Gouanvé, *Membranes*, 2021, **11**(2), 151.

79 F. Wu, M. Misra and A. K. Mohanty, *Prog. Polym. Sci.*, 2021, **117**, 101395.

80 A. M. Pinto, J. Cabral, D. A. P. Tanaka, A. M. Mendes and F. D. Magalhaes, *Polym. Int.*, 2013, **62**(1), 33–40.

81 E. L. Papadopoulou, P. Basnett, U. C. Paul, S. Marras, L. Ceseracciu, I. Roy and A. Athanassiou, *ACS Omega*, 2019, **4**(22), 19746–19755.

82 P. G. Ren, X. H. Liu, F. Ren, G. J. Zhong, X. Ji and L. Xu, *Polym. Test.*, 2017, **58**, 173–180.

83 J. Ambrosio-Martín, G. Gorrasi, A. Lopez-Rubio, M. J. Fabra, L. C. Mas, M. A. López-Manchado and J. M. Lagaron, *J. Appl. Polym. Sci.*, 2015, **132**(29), 42217.

84 H. Xu, L. Xie, D. Wu and M. Hakkarainen, *ACS Sustainable Chem. Eng.*, 2016, **4**(4), 2211–2222.

85 P. Dhar, U. Bhardwaj, A. Kumar and V. Katiyar, *Polym. Eng. Sci.*, 2015, **55**(10), 2388–2395.

86 A. K. Pal and V. Katiyar, *Biomacromolecules*, 2016, **17**(8), 2603–2618.

87 E. L. Papadopoulou, U. C. Paul, T. N. Tran, G. Suarato, L. Ceseracciu, S. Marras, *et al.*, *ACS Appl. Mater. Interfaces*, 2019, **11**(34), 31317–31327.

88 J. Xu, P. H. Manepalli, L. Zhu, S. Narayan-Sarathy and S. Alavi, *J. Polym. Res.*, 2019, **26**, 1–10.

89 J. H. Chang, Y. U. An and G. S. Sur, *J. Polym. Sci., Part B: Polym. Phys.*, 2003, **41**(1), 94–103.

90 M. D. Sanchez-Garcia and J. M. Lagaron, *J. Appl. Polym. Sci.*, 2010, **118**(1), 188–199.

91 J. Vandewijngaarden, R. Wauters, M. Murariu, P. Dubois, R. Carleer, J. Yperman, *et al.*, *J. Polym. Environ.*, 2016, **24**, 104–118.

92 P. Maiti, K. Yamada, M. Okamoto, K. Ueda and K. Okamoto, *Chem. Mater.*, 2002, **14**(11), 4654–4661.

93 S. S. Ray, K. Yamada, M. Okamoto, A. Ogami and K. Ueda, *Chem. Mater.*, 2003, **15**(7), 1456–1465.

94 N. Tenn, N. Follain, J. Soulestin, R. Crétois, S. Bourbigot and S. Marais, *J. Phys. Chem. C*, 2013, **117**(23), 12117–12135.

95 W. L. Tham, B. T. Poh, Z. A. M. Ishak and W. S. Chow, *J. Therm. Anal. Calorim.*, 2016, **126**, 1331–1337.

96 A. B. Kharissova, O. V. Kharissova, B. I. Kharisov and Y. P. Méndez, *Nano-Struct. Nano-Objects*, 2024, **37**, 101100.

© 2025 The Author(s). Published by the Royal Society of Chemistry

RSC Appl. Polym., 2025, **3**, 1244–1257 | **1257**